ARMY RESEARCH LABORATORY

Investigating the Use of Ultrasonic Guided Wave Analysis Methods for Detecting and Classifying a Small Notch in a Thin Metallic Plate

by Robert F. Anastasi

ARL-TR-5432 **February 2011**

Approved for public release; distribution is unlimited.

NOTICES

Disclaimers

The findings in this report are not to be construed as an official Department of the Army position unless so designated by other authorized documents.

Citation of manufacturer's or trade names does not constitute an official endorsement or approval of the use thereof.

Destroy this report when it is no longer needed. Do not return it to the originator.

Army Research Laboratory
Aberdeen Proving Ground, MD 21005-5066

ARL-TR-5432 **February 2011**

Investigating the Use of Ultrasonic Guided Wave Analysis Methods for Detecting and Classifying a Small Notch in a Thin Metallic Plate

Robert F. Anastasi
Vehicle Technology Directorate, ARL

Approved for public release; distribution is unlimited.

REPORT DOCUMENTATION PAGE	Form Approved OMB No. 0704-0188

Public reporting burden for this collection of information is estimated to average 1 hour per response, including the time for reviewing instructions, searching existing data sources, gathering and maintaining the data needed, and completing and reviewing the collection information. Send comments regarding this burden estimate or any other aspect of this collection of information, including suggestions for reducing the burden, to Department of Defense, Washington Headquarters Services, Directorate for Information Operations and Reports (0704-0188), 1215 Jefferson Davis Highway, Suite 1204, Arlington, VA 22202-4302. Respondents should be aware that notwithstanding any other provision of law, no person shall be subject to any penalty for failing to comply with a collection of information if it does not display a currently valid OMB control number.
PLEASE DO NOT RETURN YOUR FORM TO THE ABOVE ADDRESS.

1. REPORT DATE *(DD-MM-YYYY)*	2. REPORT TYPE	3. DATES COVERED (From - To)
February 2011	Final	4 March 2010–26 August 2010

4. TITLE AND SUBTITLE
Investigating the Use of Ultrasonic Guided Wave Analysis Methods for Detecting and Classifying a Small Notch in a Thin Metallic Plate

5a. CONTRACT NUMBER

5b. GRANT NUMBER

5c. PROGRAM ELEMENT NUMBER

6. AUTHOR(S)
Robert F. Anastasi

5d. PROJECT NUMBER

5e. TASK NUMBER

5f. WORK UNIT NUMBER

7. PERFORMING ORGANIZATION NAME(S) AND ADDRESS(ES)
U.S. Army Research Laboratory
ATTN: RDRL-VTM
NASA Langley Research Center
Hampton, VA 23681

8. PERFORMING ORGANIZATION REPORT NUMBER
ARL-TR-5432

9. SPONSORING/MONITORING AGENCY NAME(S) AND ADDRESS(ES)

10. SPONSOR/MONITOR'S ACRONYM(S)

11. SPONSOR/MONITOR'S REPORT NUMBER(S)

12. DISTRIBUTION/AVAILABILITY STATEMENT
Approved for public release; distribution is unlimited.

13. SUPPLEMENTARY NOTES

14. ABSTRACT
Aircraft and rotorcraft structures are being redesigned with new lower weight materials; however, older metallic structures continue to be used. These older structures need monitoring and characterization of damage for continued operation. The use of ultrasonic guided waves is one nondestructive technique that can be used to interrogate such structures. Typically, large cracks or geometric variations can be found by examining signal amplitude; but smaller damage that can suddenly grow in size and causes serious damage cannot be detected. This work investigates the detection and characterization of such damage where ultrasonic guided waves are transmitted across damage (a notch) in a metallic plate and numerically examined. Data is generated for a rectangular notch of varying depth and position using a finite-difference model and analyzed in time, frequency, and combined time frequency. Results show that a small notch, 0.1 mm deep, cannot be detected using conventional time or frequency domain analysis but can be detected using time-frequency representations.

15. SUBJECT TERMS
guided waves, time, frequency, time-frequency, analysis, damage, notch

16. SECURITY CLASSIFICATION OF:			17. LIMITATION OF ABSTRACT	18. NUMBER OF PAGES	19a. NAME OF RESPONSIBLE PERSON
a. REPORT	b. ABSTRACT	c. THIS PAGE			Robert F. Anastasi
Unclassified	Unclassified	Unclassified	UU	22	19b. TELEPHONE NUMBER (*Include area code*) 757-864-3391

Standard Form 298 (Rev. 8/98)
Prescribed by ANSI Std. Z39.18

Contents

List of Figures

1. Introduction

Guided Lamb wave nondestructive evaluation is a tool used in structural health monitoring of aircraft, civil, and mechanical infrastructures. The goal is to determine how wave velocity and mode shape are influenced by changes in geometry and/or boundary conditions caused by structural damage or degradation. These waves propagate in thin plates and plate-like structures and are formed by the interference of multiple reflections and mode conversions of longitudinal and shear waves at the plate surfaces. Guided waves are typically generated and detected using conventional piezoelectric transducers, oriented either flat or at an angle with respect to the surface. Two types of waves propagate a symmetric wave and an antisymmetric wave, each with multiple modes and at different frequency and speeds that complicate data analysis. To avoid analysis complications, fundamental symmetric (S_0) and antisymmetric (A_0) modes at low-frequency thickness values are typically used for inspections by limiting source transducer bandwidth. Processing and analysis of guided wave signals are typically performed in the time and frequency domain. Other popular analysis methods include integrated time-frequency domain and wavelet analysis. In some cases, baseline signals are subtracted from inspection signals to enhance results.

A wide range of work has been reported on the interaction of guided waves (Lamb waves) with damage. In these works, the majority of analysis was done through examining transmission and reflection coefficients. For example, Lamb wave interaction with straight sided notches was investigated by Alleyne and Cawley (*1*) through a finite-element model and two-dimensional (2-D) Fourier analysis of low-order modes. Their results showed that the reflection and transmission coefficients of individual Lamb wave modes to notch geometry and orientation are dependent on frequency, plate, and wave mode. Lowe et al. (*2*) and Lowe and Diligent (*3*) also investigated Lamb wave interaction with a rectangular notch for first-order symmetric and antisymmetric modes. They used reflection coefficients to quantify results that showed a sharp rise in reflection coefficient for a notch depth-to-plate thickness of 50% and greater. Benmeddour et al. (*4*) used a method to predict the propagation of fundamental Lamb wave modes in an isotropic structure containing symmetric notches; power reflection and transmission coefficients were used in his analysis. Differential guided wave features were used by Michaels et al. (*5*) to classify structural changes such as holes and temperature variations. Classifiers utilizing time and frequency domain features were compared to classifications based on time-frequency representations. Both classification schemes were able to discriminate between environmental and structural changes in a small aluminum plate. In this report, guided waves transmitted across a notch (simulated damage) in a metallic plate are numerically generated and examined with various analysis methods to determine the wave defect sensitivity and potential damage characterization.

2. Fundamental of Lamb Waves

Guided waves or Lamb waves are formed by the interference of multiple reflections and mode conversions of longitudinal and shear waves at the free surfaces of a plate. These waves are typically generated and detected using conventional piezoelectric transducers, oriented either flat or at an angle with respect to the surface, and are used to detect defects and measure elastic properties of thin isotropic materials and laminated composite plates. Two types of waves propagate a symmetric wave and an antisymmetric wave. Each of these wave types propagates with multiple modes.

By solving a boundary value problem for a free plate or by considering the reflection of waves at plate boundaries, the Rayleigh-Lamb frequency equations (dispersion equations) can be found (*6*–*9*). For a uniform traction-free isotropic plate, the equation for symmetric modes is

$$\frac{\tan(qh)}{\tan(ph)} = -\frac{4\,k^2 pq}{\left(q^2 - k^2\right)^2}\,. \tag{1}$$

For antisymmetric modes,

$$\frac{\tan(qh)}{\tan(ph)} = -\frac{\left(q^2 - k^2\right)^2}{4\,k^2 pq}\,, \tag{2}$$

where

$$p^2 = \frac{\omega^2}{c_L^2} - k^2\,,\; q^2 = \frac{\omega^2}{c_T^2} - k^2\,, \text{ and } k = \omega/c_P\,, \tag{3}$$

and h, k, c_L, c_T, c_P, and ω are the half-plate thickness, wave number, velocities of longitudinal and transverse modes, phase velocity, and wave circular frequency, respectively.

The phase velocity is found numerically by solving the real roots of the dispersion equation as a function of material properties, frequency, and material thickness. Group velocity dispersion curves are found from the phase velocity (*9*).

Phase and group velocity dispersion curves for a 2.0-mm-thick aluminum plate are shown in figure 1, where longitudinal velocity (c_L), transverse velocity (c_T), and density (ρ) of the plate are equal to 6420 m/s, 3040 m/s, and 2700 kg/m^3, respectively. These curves were generated and plotted using a commercial software package (*10*).

The figure shows the first three symmetric and antisymmetric mode dispersion curves. At low frequencies, the wave velocity of the first symmetric mode (S_0) is nearly nondispersive, while the wave velocity of the first antisymmetric mode (A_0) is highly dispersive. At higher frequencies, phase velocity of both zero-order modes approaches the Rayleigh wave velocity, $c_{R,}$ which has a value of ~2.9 km/s (*6*) for aluminum with a Poisson's ratio $\nu = 0.33$.

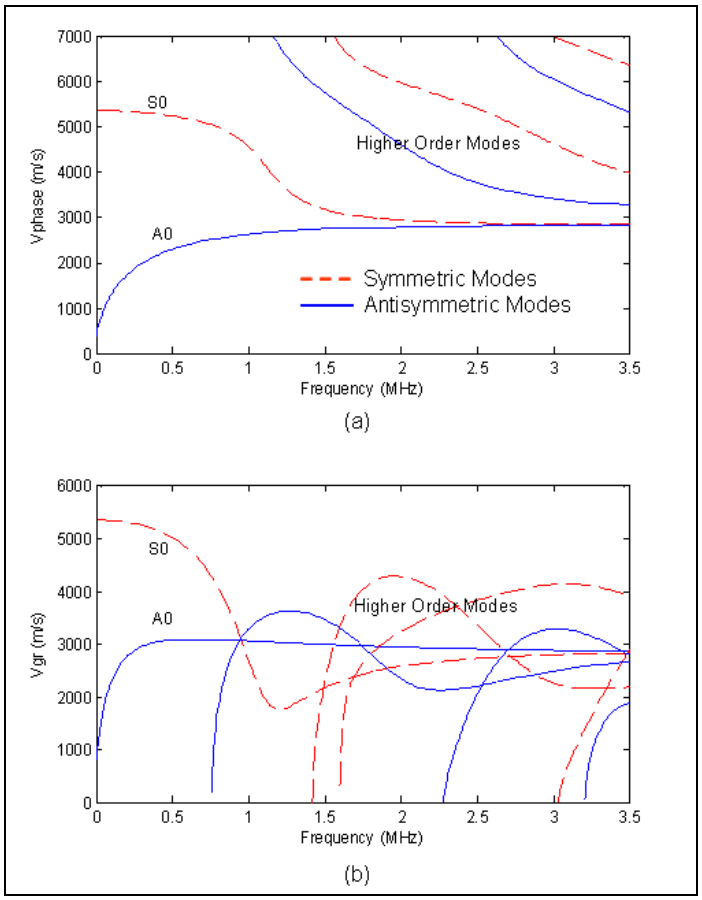

Figure 1. Dispersion curves for 2.0-mm-thick aluminum plate (a) phase velocity and (b) group velocity vs. frequency, where S0 and A0 are first-order symmetric and antisymmetric modes, respectively.

3. Finite-Difference Model and Simulations

A finite-difference model was used to simulate wave propagation in a thin aluminum plate with notch. For this modeling and simulation, commercial software (*11*) was used based on a published algorithm (*12*) that solves a 2-D (plane strain) acoustic wave equation. A schematic diagram of the finite-difference time domain model is shown in figure 2. In the model, the ultrasonic source and receiver were each 10 mm in diameter and in planar contact with the sample surface positioned 100 mm apart. The aluminum plate was 2.0 mm thick and 600 mm wide. A wide width was used to prevent interference of edge reflections. Aluminum properties of the material used in the model were longitudinal velocity of 6420 m/s, transverse velocity of 3040 m/s, and density of 2700 kg/m^3. The simulated damage (the notch) had a width of 6.0 mm and depth from the sample back surface that ranged from 0.0 to 1.0 mm in 0.1-mm steps. Notch depth translated to a depth-to-thickness ratio of 0% to 50%. To vary the location of the notch, the source and receiver transducers were repositioned but always kept 100 mm apart. For example, the notch was centered at 0.0 along the axis, the source was positioned at –40 mm, and the receiver positioned at 60 mm.

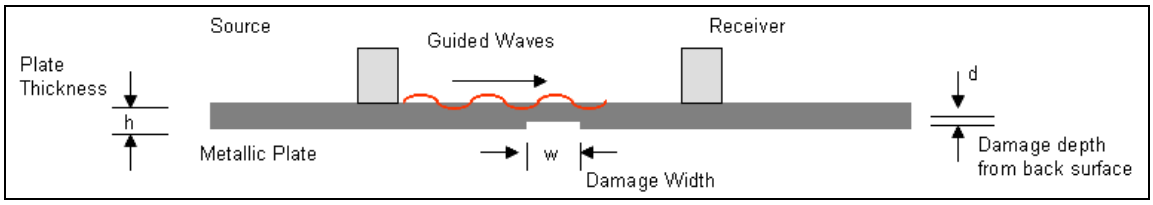

Figure 2. Finite-difference model schematic.

Two different transmitter or source signals were used. A sine Gaussian pulse and sine exponential pulse were available as functions in the software. Source signals and spectrums for the sine Gaussian pulse and sine exponential pulse are shown in figures 3 and 4, respectively. The sine Gaussian pulse spectrum has a full-width-half-height (FWHH) bandwidth of ~0.32 MHz and ranges from 0.0 to 1.0 MHz. The sine exponential pulse spectrum has a FWHH bandwidth of ~0.43 MHz and frequency range from 0.0 to ~2.0 MHz, with low amplitude frequency components above 1 MHz.

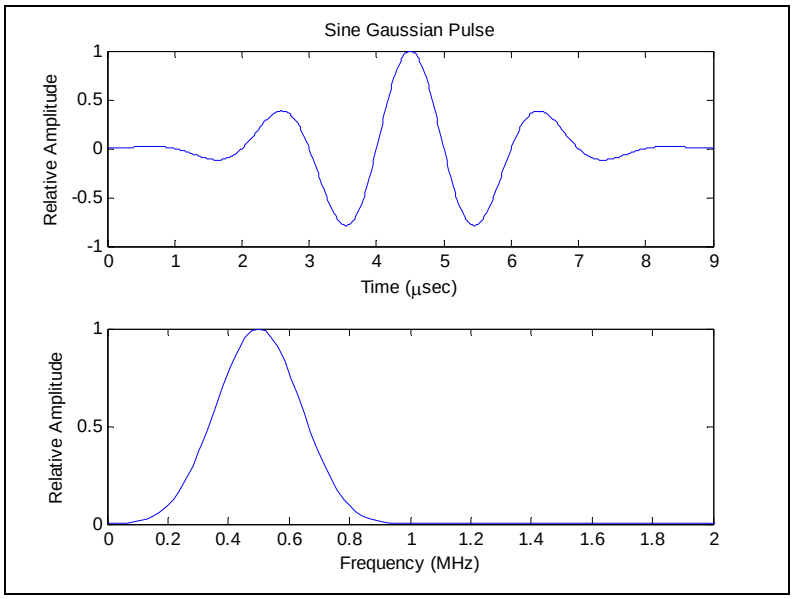

Figure 3. Sine Gaussian function and its spectrum used in the simulation as a source function.

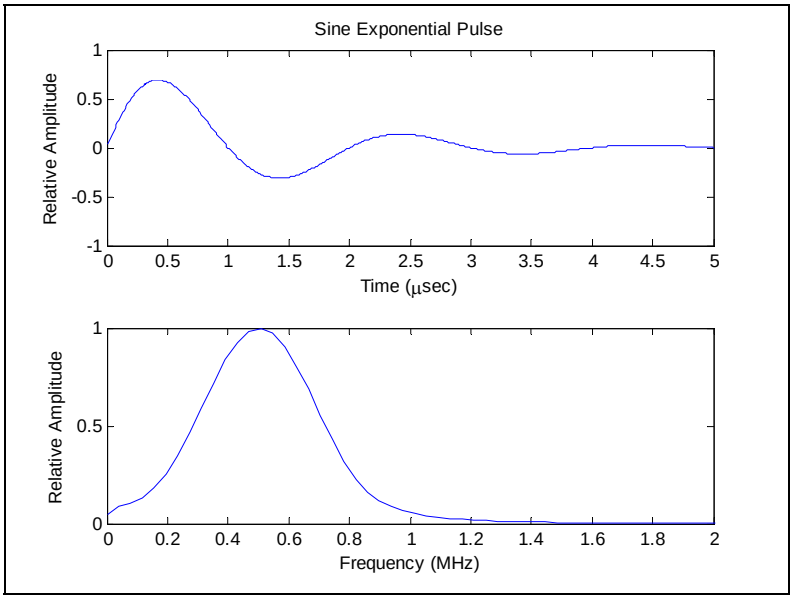

Figure 4. Sine exponential function and its spectrum used in the simulation as a source function.

Example temporal snapshots of guided waves propagation in the sample with a centrally located notch are shown in figure 5. This figure shows how the wave spreads as a function of time. An example receiver signal is shown in figure 6, where figure 6a shows a signal for no damage (or baseline) and figure 6b shows a signal for a centrally located notch with a 0.5 mm deep. For these signals, the S_0 mode is located at ~20 μs and the A_0 mode starts at ~30 μs. A series of signals were generated for various notch depth and position and were examined in time, frequency, and time-frequency domains.

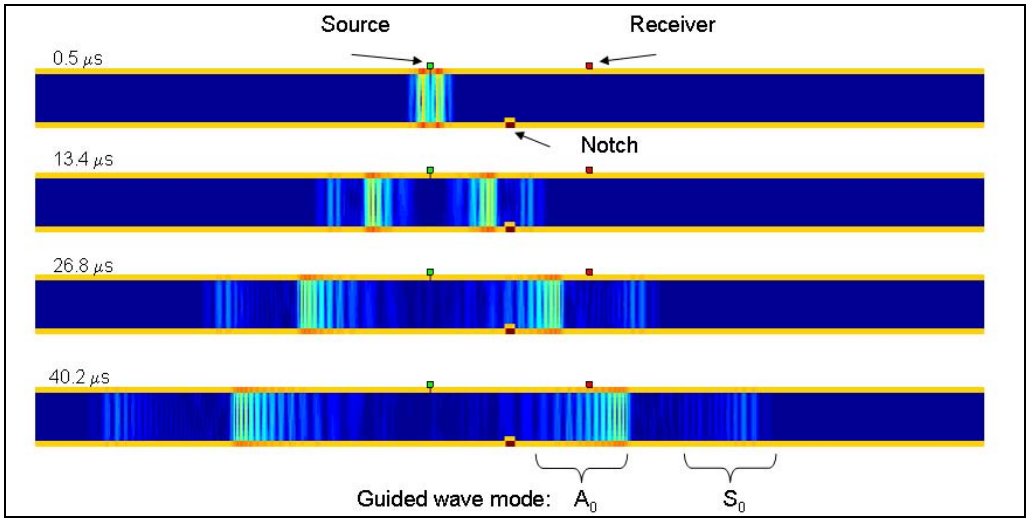

Figure 5. Typical snapshots of the guided wave propagating in the model.

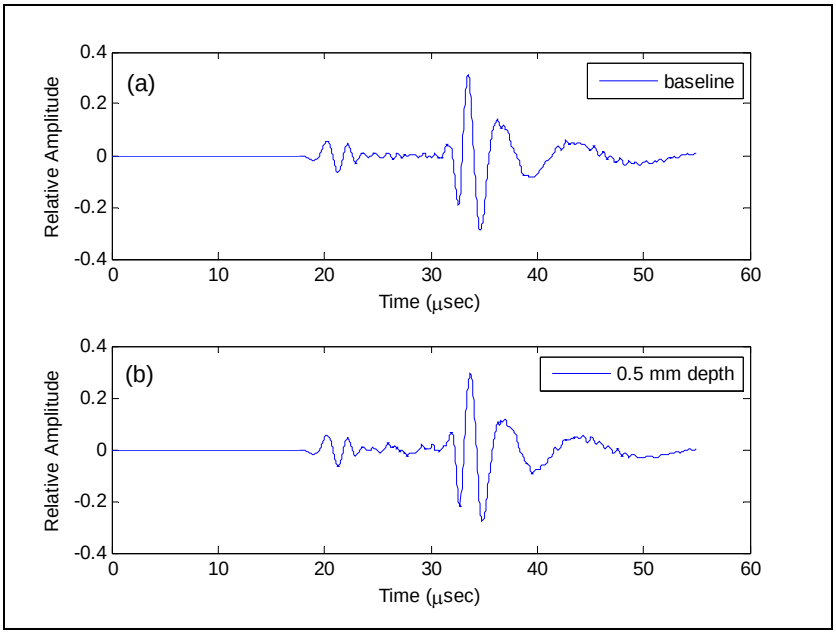

Figure 6. Simulated time-domain signal showing the primary symmetric and antisymmetric modes for (a) baseline signal without damage and (b) a notch with 0.5-mm depth. (Source signal was a sine exponential pulse.)

4. Time and Frequency Analysis and Results

Time and frequency domain analysis of signals similar to the ones shown in figure 6 was performed. In this analysis, wave transmission coefficients, Fourier-transform magnitude, spectral energy, and average powered vs. notch depth were considered. The A_0 and S_0 mode transmission coefficients were obtained by dividing the subject mode amplitude by its corresponding baseline amplitude. The A_0 mode transmission coefficient over a range of notch depth is shown in figure 7a and shows an almost constant value to a notch depth of about 0.5 mm and decreasing values for deeper notch depths. A plot of transmission coefficients for the S_0 mode in figure 7b shows a similar result. Spectral analysis for a series of notch depths is shown in figure 8. The Fourier-transform magnitude is shown in figure 8a. Overall, the magnitude trend is difficult to determine, but, in general, there is a decreasing magnitude for increasing notch depth. The spectral energy in figure 8b also shows decreasing energy for increasing notch depth. Average signal power as a function of notch depth is shown in figure 9. This shows a similar trend as depicted in figures 7–9. These plots showed time or frequency aspect of a guided wave signal vs. notch depth. They showed a flat response or no change in signal amplitude, spectral magnitude, and average power up to a damage depth of ~0.5 mm (25% of material thickness), making them insufficient to determine shallow notch depth.

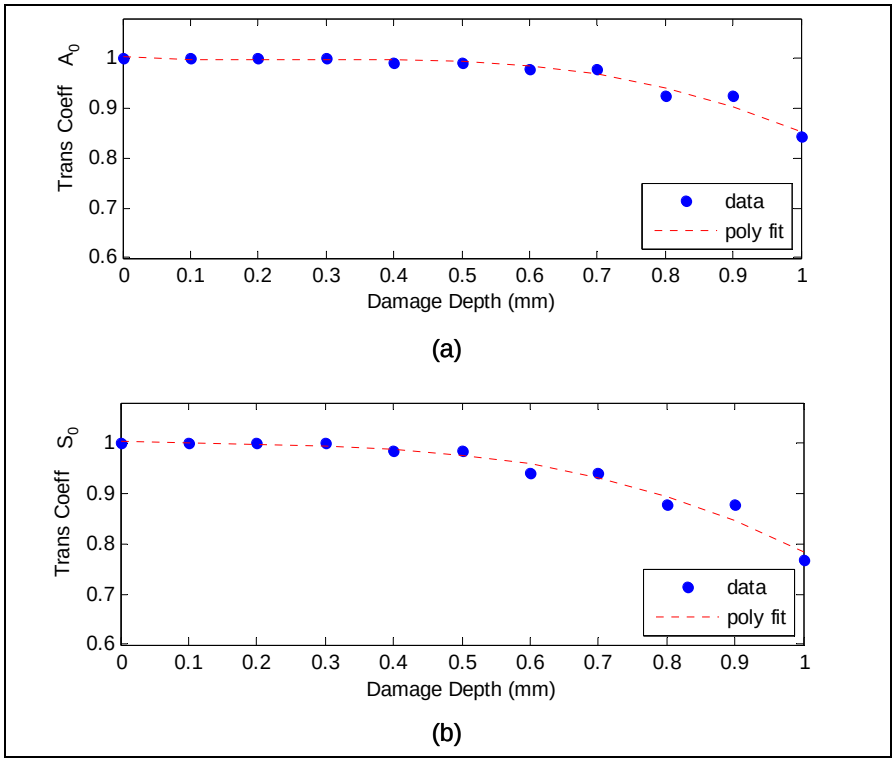

Figure 7. Transmission coefficient for (a) A_0 mode vs. notch depth and (b) S_0 mode vs. notch depth.

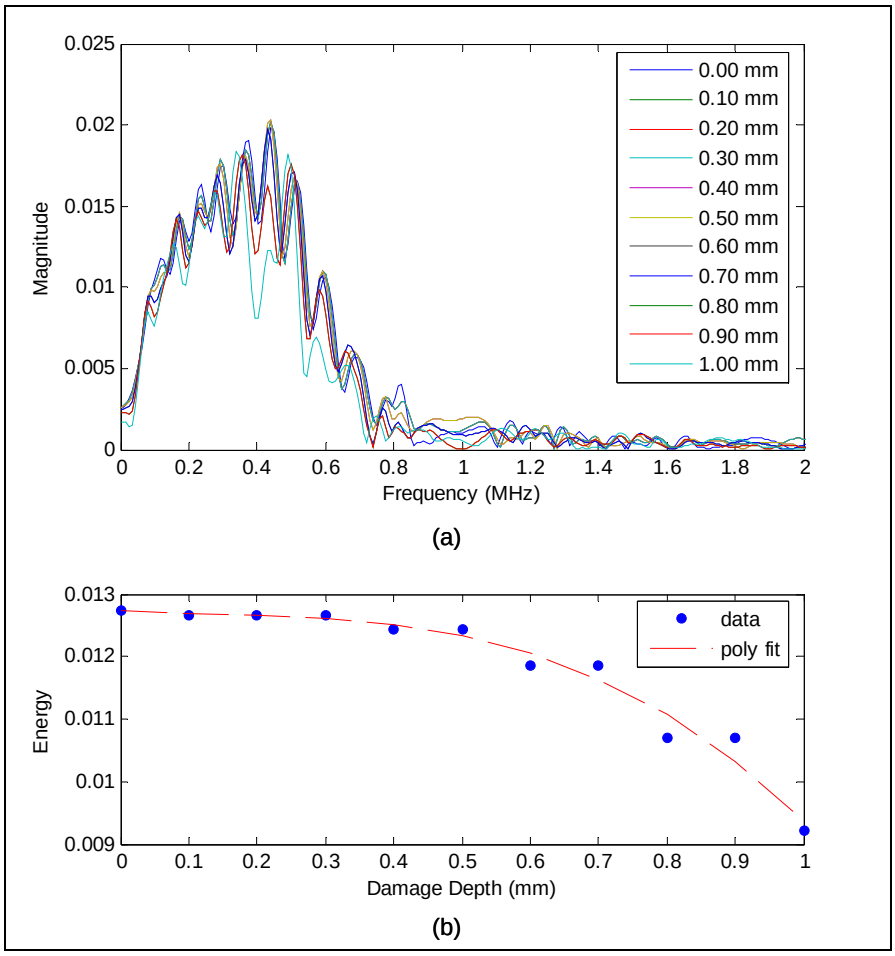

Figure 8. Spectral analysis of signal shows (a) the Fourier-transform magnitude vs. notch depth and (b) spectral energy vs. notch depth.

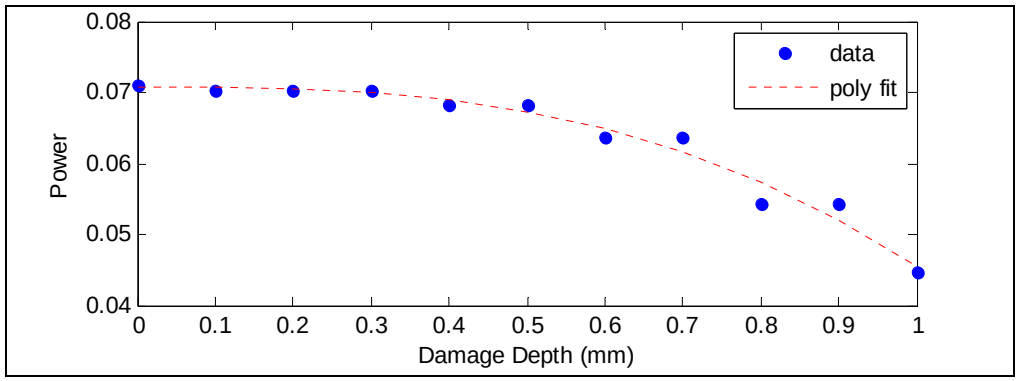

Figure 9. Average power vs. notch depth.

5. Integrated Time-Frequency Analysis and Results

A time-frequency representation (TFR) (*13*) is another method used for signal analysis. It has been used to identify Lamb wave modes and dispersion curves which, in turn, can be used to calculate material properties. The TFR maps a one-dimensional time-domain signal into a 2-D function of time and frequency displayed as a gray-scale or false-color image. The TFR used here is the short-time Fourier transform (STFT) or its magnitude squared the spectrogram and the reassigned spectrogram (*14–19*).
For reference, the STFT is as follows (*20*):

$$\mathrm{STFT}\{x(t)\} \equiv X(\tau,\omega) = \int_{-\infty}^{\infty} x(t)\,\omega(t-\tau)\,e^{-j\omega t}\,dt\,, \tag{4}$$

where $\omega(t)$ is the window function, typically a Hann, Hamming, or Gaussian window, and $x(t)$ is the signal to be transformed. The spectrogram, the STFT magnitude squared, is as follows (*20*):

$$\mathrm{spectrogram}\{x(t)\} \equiv \left|X(\tau,\omega)\right|^2\,. \tag{5}$$

Spectrogram resolution depends on the window size, type, and overlap. The width of the window relates to frequency resolution (the separation of frequency components) or time resolution (the time at which frequencies change). A wide window gives better frequency resolution but poor time resolution. A narrow window gives good time resolution but poor frequency resolution. As a result, a tradeoff exists between improved time and frequency resolution. The reassigned spectrogram sharpens time and frequency estimates and thus can be considered a postprocessing on the STFT distribution for improve readability. One reassignment method (*18, 19, 21*) uses a moving window to maximize the coefficients in a local time-frequency distribution, and another method (*22*) uses results of two STFTs with slightly modified window functions.

The signals in figure 6 with and without damage (notch depth of 0.5 mm or 25% of material thickness) were mapped to the time-frequency domain. The spectrogram for the baseline signal in figure 6a is shown in figure 10a. In this spectrogram, the dispersion group velocity curves the S_0, S_1, A_0, and A_1 modes) from figure 1b are superimposed over the time-frequency map and illustrate the time-frequency and group velocity mapping for the given source bandwidth. Dispersion curve group velocity was converted to time using the source receiver separation distance as a conversion parameter. The intensity map shows the primary A_0 and S_0 Lamb wave modes and some higher modes, with the S_0 mode arriving at about 18 μs and the A_0 mode arriving at about 30 μs. Frequency dispersion of the A_0 can be seen with the higher frequency modes arriving before the lower frequency modes. The spectrogram for the signal with damage is shown in figure 10b. This figure is similar to figure 10a except that the region between the S_0 and A_0 modes at about 25 μs shows a mode conversion resulting from the notch.

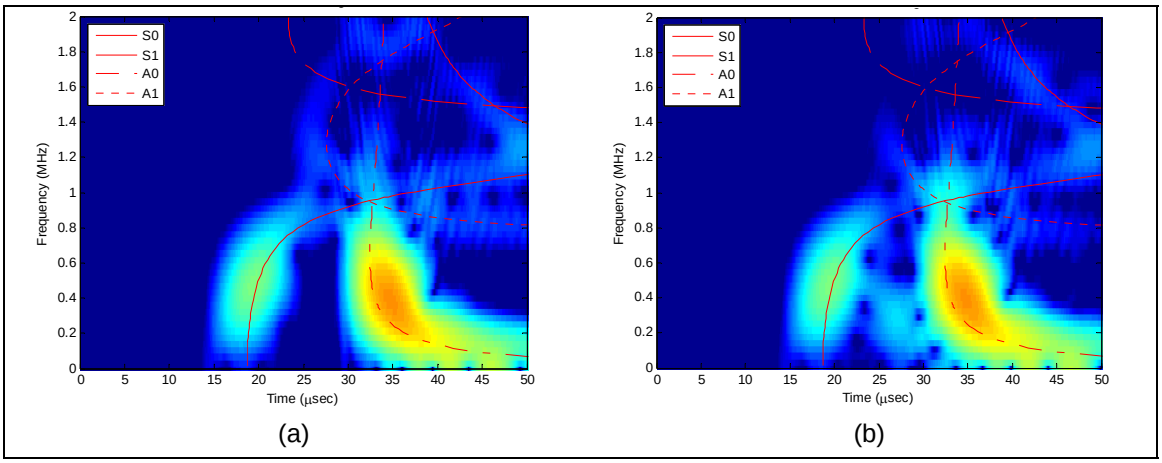

Figure 10. Spectrogram for (a) baseline signal and (b) signal with 0.5-mm-deep notch for a sine exponential source signal.

To see the result of a different source signal, simulated signals were generated for the same geometry as the ones shown in figure 6, but with a sine Gaussian source function. The result mapped to the time-frequency domain in figure 11 shows a reduced bandwidth as a result of the source signal. As in figure 10, figure 11 shows the mode conversion from the notch in the area between the S_0 and A_0 modes.

When a reassigned spectrogram was applied, the TFR coefficients in figures 10 and 11 follow the dispersion curves along a tighter focus. These results are shown in figures 12 and 13 for the sine exponential and sine Gaussian pulse, respectively. Although these results show a tighter focus, the reassignment process dissipates and the mode converts the signal, making the reassignment spectrogram less useful for the current purpose.

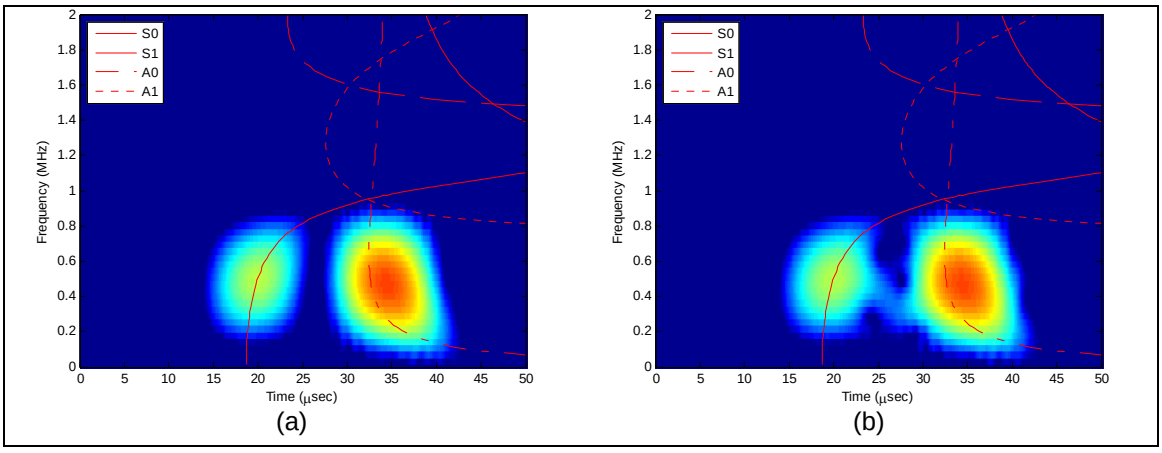

Figure 11. Spectrogram for (a) baseline signal and (b) signal with 0.5-mm-deep notch for a sine Gaussian source signal.

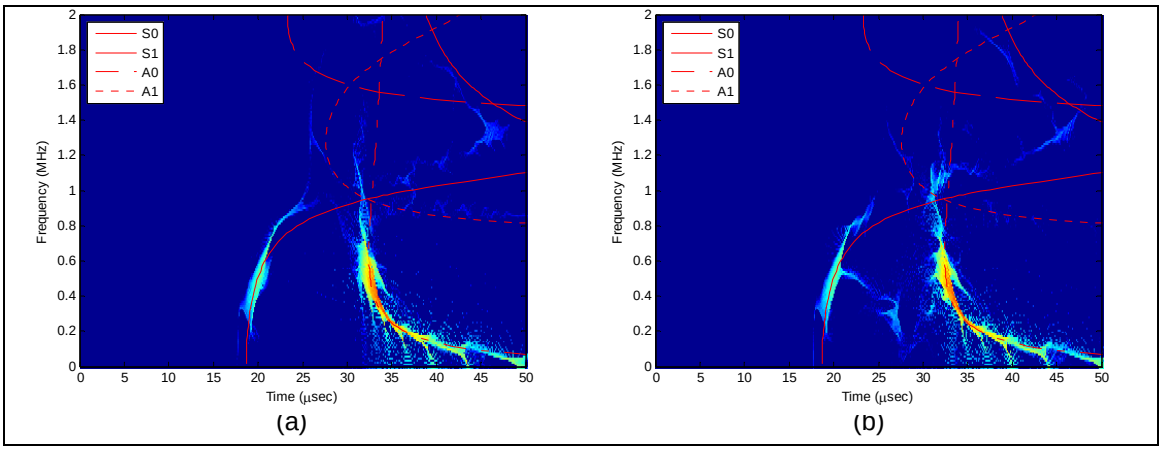

Figure 12. Reassigned spectrogram for (a) baseline signal and (b) signal with 0.5-mm-deep notch for a sine exponential source signal.

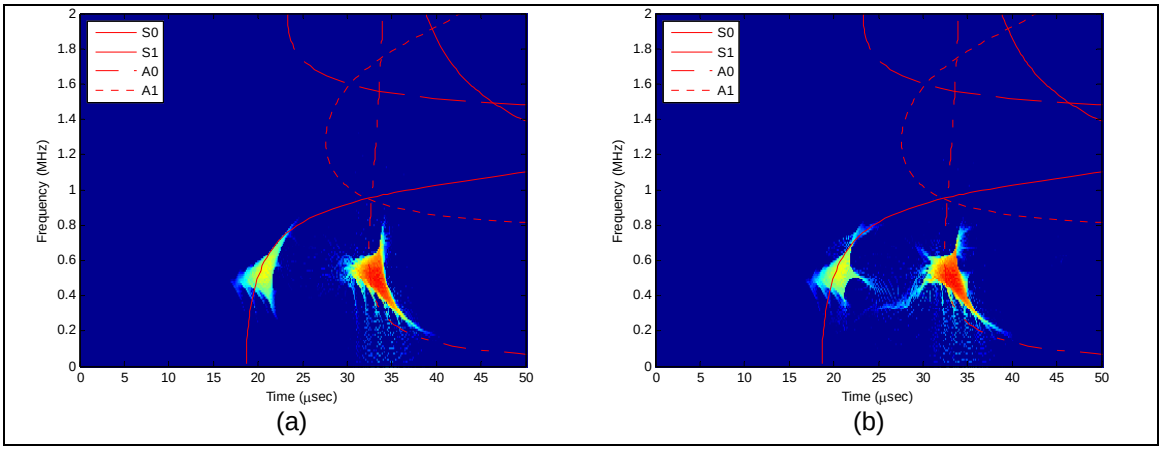

Figure 13. Reassigned spectrogram for (a) baseline signal and (b) signal with 0.5-mm-deep notch for a sine Gaussian source signal.

Damage or notch sensitivity was examined through the spectrogram by processing guided wave signals generated for a series of notch depths and the sine exponential source signal, which has a larger bandwidth than the sine Gaussian source signal. Of the smaller notched depths examined 0.05 and 0.10 mm deep, only the latter showed the effect of the mode conversion. The spectrogram for the 0.10-mm notch is shown in figure 14a, and a 0.9-mm notch is shown in figure 14b. The result is similar to figure 10b, with the mode converted signal appearing at about 25 μs. Comparing the mode-converted signal in figures 10b and 14, it appears that the intensity of the mode-converted signal is increasing. However, when the intensity was examined for the series of notch depths, the mode-converted signal intensity did not consistently increase as depth increased. This was most likely due to wave addition and subtraction and, thus, varying wave intensity.

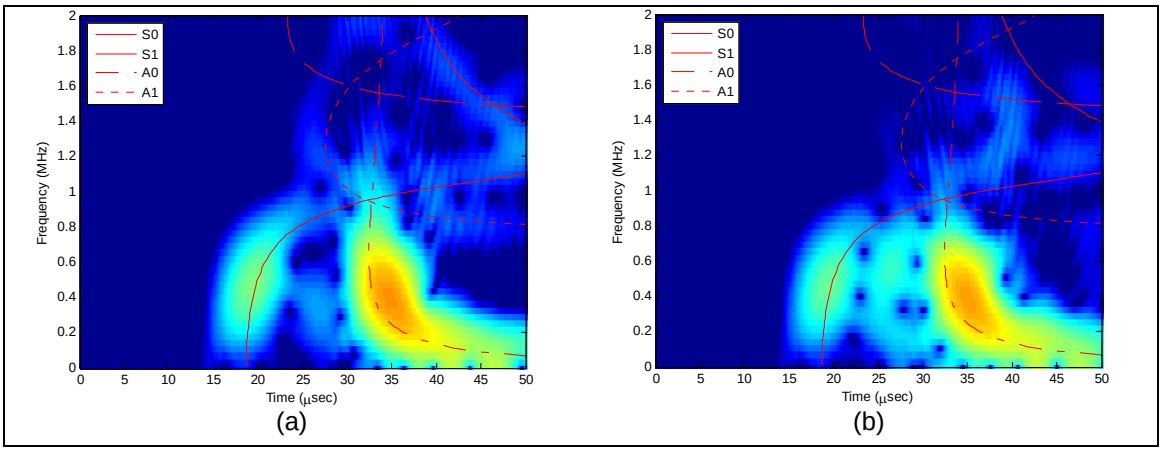

Figure 14. Spectrogram for a signal with (a) 0.1-mm and (b) 0.9-mm-deep notch and sine exponential source signal.

The damage or notch for the spectrogram images was centered between the source and receiver. When the notch was offset from the center, the temporal location of the mode converted signal shifted. Figure 15 shows spectrograms for a 0.1-mm-deep notch centered in figure 15a, offset 10 mm in figure 15b, and offset 20 mm in figure 15c. In this sequence, the temporal location of the mode converted signal in figure 15a–c moves from ~25, to 27, to 29 μs, respectively. These temporal locations are difficult to determine accurately because the spectrogram's S_0 and A_0 mode components are broad and fuzzy.

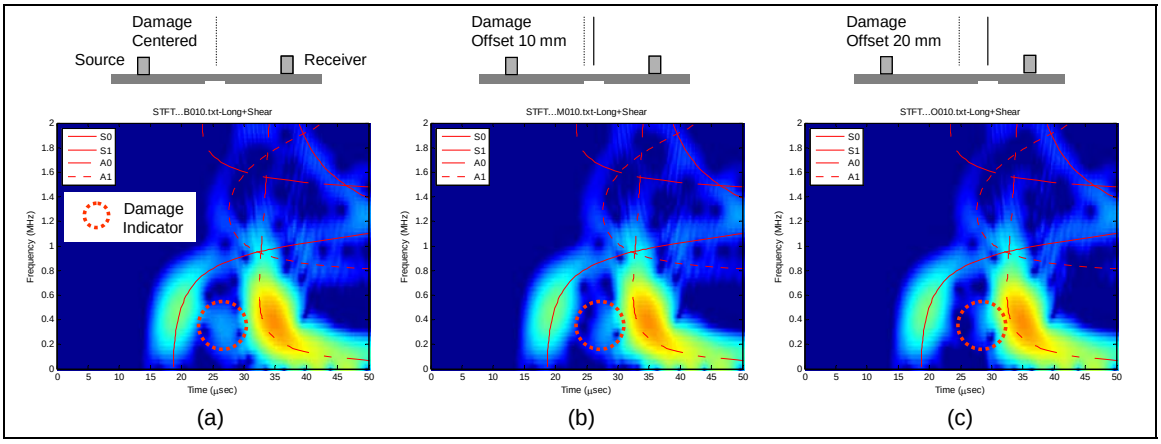

Figure 15. Damage indicator temporal location as a function of a 0.1-mm-deep notch physical location between the source and receiver (a) centered or no offset, (b) 10-mm offset, and (c) 20-mm offset, with damage temporal locations of ~25, 27, and 29 μs, respectively.

6. Conclusions

Time, frequency, and time-frequency analysis methods of ultrasonic guided waves for detecting a small notch were present. Ultrasonic-guided wave signals were numerically generated using a finite-difference model. In this model, damage was simulated in a rectangular notch of varying depth and position between a source and receiver transducer. The signals displayed the classical symmetric and antisymmetric modes. Analysis of these signals as a function of notch depth showed a flat response or no change in signal amplitude, spectral magnitude, and average power up to a damage depth of ~0.5 mm (or 25% of the sample thickness). For greater damage or notch depths, larger changes were observed. This result showed that gross damage could be detected, but not shallow damage less than 25% of material thickness.

Time-frequency representation of signals was more successful in displaying signal changes due to shallow depth damage. Spectrogram images displayed artifacts from the notch for shallow depths as small as 0.1 mm (or 5% of sample thickness). Of the two source waveforms used, the sine exponential pulse showed a better localization of signal artifacts from the notch, although this may be an effect of image intensity settings. The reassigned spectrogram focused the time-frequency data tighter along the dispersion curves but seemed to dissipate the data from the notch as a result of the reassignment algorithm; this was not beneficial to the analysis. Spectrogram sensitivity to the notch position was examined. This illustrated that the notch could be tracked to a temporal position between the source and receiver, but accuracy was poor due to the cloud nature of the TFR.

Overall, the time-frequency representation displayed signal variations due to a shallow notch depth as small as 0.1 mm, 5% of material thickness which is 5× smaller than what could be detected by time and frequency analysis methods alone. Thus, TFR methods can be used to interrogate a structure and detect small damage which can then be repaired to prevent serious damage to equipment and personnel.

7. References

1. Alleyne, D. N.; Cawley, P. The Interaction of Lamb Waves with Defects. *IEEE Transactions on Ultrasonics, Ferroelectronics, and Frequency Control* **1992**, *39* (3), 381–397.

2. Lowe, M. J. S.; Cawley, P.; Kao, J.-K.; Diligent, O. The Low Frequency Reflection Characteristics of the Fundamental Antisymmetric Lamb Wave A0 from a Rectangular Notch in a Plate. *J. Acoustic Soc. Am.* **2002**, *112* (6), 2612–2622.

3. Lowe, M. J. S.; Diligent, O. Low-Frequency Reflection Characteristics of the S0 Lamb Wave from a Rectangular Notch in a Plate. *J. Acoustic Soc. Am.* **2002**, *111* (1), 64–74.

4. Benmeddour, F.; Grondel, S.; Assaad, J.; Moulin, E. Study of the Fundamental Lamb Modes Interaction with Symmetrical Notches. *NDT&E International* **2008**, *41*, 1–9.

5. Michaels, J. E.; Cobb, A. C.; Michaels, T. E. A Comparison of Feature-Based Classifiers for Ultrasonic Structural Health Monitoring, Health Monitoring and Smart Nondestructive Evaluation of Structural and Biological Systems III. Kundu, T., Ed.; *Proc. SPIE*, 2004; Vol. 5394, pp 363–374.

6. Auld, B. A. *Acoustic Fields and Waves in Solids*; Robert E. Krieger Publishing Company, 1990, Vol. 2.

7. Achenbach, J. D. *Wave Propagation in Elastic Solids*; Elsevier Science Publishers: New York, 1999.

8. Viktrorov, I. A. *Rayleigh and Lamb Waves*; Plenum Press: New York, 1967.

9. Rose, J. L. *Ultrasonic Waves in Solid Media*; Cambridge University Press: New York, 1999.

10. Pavlakovic, B.; Lowe, M. J. S. Disperse, An Interactive Program for Generating Dispersion Curves; Imperial College NDT Lab: London, UK, 2001.

11. Cyberlogic, Inc. *Wave2000, v1.00a*. A stand-alone computer software program for computational ultrasonics; New York, NY, 1997.

12. Schechter, R. S.; Chaskelis, H. H.; Mignogna, R. B.; Delsanto, P. P. Real-time Parallel Computation and Visualization of Ultrasonic Pulses in Solids. *Science* **1994**, *265*, 1188–92.

13. Wikipedia, The Free Encyclopedia. Time-Frequency Representation. http://en.wikipedia.org/w/index.php?title=Time%E2%80%93frequency_representation&oldid=377119454 (accessed 2010).

14. Niethammer, M. L.; Eisenhardt, C.; Jacobsa, L. J.; Jarzynski, J.; Qu, J. Application of the Short Time Fourier Transform to Interpret Ultrasonic Signals. *Review of Progress in Quanatative Evaluation.* Thompson, D. O., Chimenti, E. E., Eds.; American Institute of Physics, 1999, Vol. 19A, pp 703–708.

15. Niethammer, M. L.; Jacobsa, J.; Qu, J.; Jarzynski, J. Time-Frequency Representation of Lamb Waves Using the Reassigned Spectrogram. *J. Acoust. Soc. Am.* **2000**, *107* (5), L19-L24.

16. Niethammer, M. L.; Jacobsa, J.; Qu, J.; Jarzynski, J. Time-Frequency Representations of Lamb Waves. *J. Acoust. Soc. Am.* **2001**, *109* (5), 1841–1847.

17. Fulup, S. A.; Fitz, K. A Spectrogram for the Twenty-first Century. *Acoustics Today* **2006**, 26–33.

18. Nilsen, G. K. *Recursive Time-Frequency Reassignment*; Department of Informatics, University of Bergen: Norway, 2007.

19. Nilsen, G. K. Recursive Time-Frequency Reassignment. *IEEE Transactions on Signal Processing* **2009**, *57* (8), 3282–3287.

20. Wikipedia, The Free Encyclopedia. Short-Time Fourier Transforms. http://en.wikipedia.org/w/index.php?title=Short-time_Fourier_transform&oldid=372262413 (accessed 2010).

21. Kodera, K.; DeVilledary, C.; Gendrin, R. *A New Method for the Numerical Analysis of Non-Stationary Signals, Physics of the Earth and Planetary Interiors*; Elsevier Scientific Publishing Company: Amsterdam, 1976; Vol. 12, pp 142–150.

22. Auger, F.; Flandrin, P. Improving the Reliability of Time-Frequency and Time-Scale Representations by the Reassignment Method. *IEEE Transactions on Signal Processing*. **1995**, *43* (5), 1068–1089.

NO. OF
COPIES ORGANIZATION

1 (PDF only) DEFENSE TECHNICAL INFORMATION CTR
DTIC OCA
8725 JOHN J KINGMAN RD
STE 0944
FORT BELVOIR VA 22060-6218

1 DIRECTOR
US ARMY RESEARCH LAB
IMNE ALC HRR
2800 POWDER MILL RD
ADELPHI MD 20783-1197

1 DIRECTOR
US ARMY RESEARCH LAB
RDRL CIM L
2800 POWDER MILL RD
ADELPHI MD 20783-1197

1 DIRECTOR
US ARMY RESEARCH LAB
RDRL CIM P
2800 POWDER MILL RD
ADELPHI MD 20783-1197

1 DIRECTOR
US ARMY RESEARCH LAB
RDRL D
2800 POWDER MILL RD
ADELPHI MD 20783-1197

ABERDEEN PROVING GROUND

1 DIR USARL
RDRL CIM G (BLDG 4600)